BIOCHEMISTRY
including biophysical chemistry & molecular biology

Article

pubs.acs.org/biochemistry

Three-Dimensional Structure of the *Rhodobacter sphaeroides* RC-LH1-PufX Complex: Dimerization and Quinone Channels Promoted by PufX

Pu Qian,[†,∥] Miroslav Z. Papiz,[‡,∥] Philip J. Jackson,[†,§] Amanda A. Brindley,[†] Irene W. Ng,[†] John D. Olsen,[†] Mark J. Dickman,[§] Per A. Bullough,[†] and C. Neil Hunter*[,†]

[†]Department of Molecular Biology and Biotechnology, University of Sheffield, Western Bank, Firth Court, Sheffield S10 2TN, United Kingdom

[‡]Institute of Integrative Biology, Biosciences Building, University of Liverpool, Crown Street, Liverpool L69 7ZB, United Kingdom

[§]ChELSI Institute, Department of Chemical and Biological Engineering, University of Sheffield, Mappin Street, Sheffield, S1 3JD, United Kingdom

Supporting Information

ABSTRACT: Reaction center-light harvesting 1 (RC-LH1) complexes are the fundamental units of bacterial photosynthesis, which use solar energy to power the reduction of quinone to quinol prior to the formation of the proton gradient that drives ATP synthesis. The dimeric RC-LH1-PufX complex of *Rhodobacter sphaeroides* is composed of 64 polypeptides and 128 cofactors, including 56 LH1 bacteriochlorophyll *a* (BChl *a*) molecules that surround and donate energy to the two RCs. The 3D structure was determined to 8 Å by X-ray crystallography, and a model was built with constraints provided by electron microscopy (EM), nuclear magnetic resonance (NMR), mass spectrometry (MS), and site-directed mutagenesis. Each half of the dimer complex consists of a RC surrounded by an array of 14 LH1 $\alpha\beta$ subunits, with two BChls sandwiched between each $\alpha\beta$ pair of transmembrane helices. The N- and C-terminal extrinsic domains of PufX promote dimerization by interacting with the corresponding domains of an LH1 β polypeptide from the other half of the RC-LH1-PufX complex. Close contacts between PufX, an LH1 $\alpha\beta$ subunit, and the cytoplasmic domain of the RC-H subunit prevent the LH1 complex from encircling the RC and create a channel connecting the RC Q_B site to an opening in the LH1 ring, allowing Q/QH_2 exchange with the external quinone pool. We also identified a channel that connects the two halves of the dimer, potentially forming a long-range pathway for quinone migration along rows of RC-LH1-PufX complexes in the membrane. The structure of the RC-LH1-PufX complex explains the crucial role played by PufX in dimer formation, and it shows how quinone traffic traverses the LH1 complex as it shuttles between the RC and the cytochrome bc_1 complex.

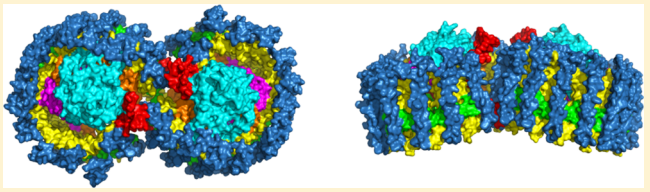

Photosynthesis, the ultimate source of all food and most bioenergy resources on Earth, begins with the absorption of solar energy by an array of antenna pigment molecules. The transfer of absorbed energy to specialized pigment−protein complexes, the reaction centers (RCs), initiates a series of electron-transfer reactions that trap the solar energy prior to its ultimate conversion to ATP, which powers the metabolism of the cell. In phototrophic bacteria, the conversion of solar energy to a chemical form, quinol, is accomplished by RC-LH1 complexes.[1,2] The largest of these pigment−proteins is the dimeric RC-LH1-PufX complex in which 28 LH1 $\alpha\beta BChl_2$ subunits form a near-continuous palisade of 56 transmembrane helices enclosing two RCs.[3] A two-way traffic of outgoing quinols and incoming quinones must traverse this LH1 barrier to allow the turnover of RC photochemistry. Once inside the confines of the encircling LH1 complex, a quinone binds to the RC Q_B site, picks up two electrons from RC photochemistry and two protons from the cytoplasm, and then exits the complex as a quinol to be replaced by a quinone from the membrane pool. The quinol migrates through the membrane bilayer to the cytochrome bc_1 complex, where a proton-motive force is generated. ATP synthase converts the proton gradient into ATP, the energy currency of the cell.

Early gene deletion experiments in the phototrophic bacteria *Rhodobacter (Rba.) sphaeroides* and *Rba. capsulatus* showed that the transmembrane PufX polypeptide facilitates quinone/quinol (Q/QH_2) exchange across the LH1 barrier.[4,5] Subsequently, other roles emerged for PufX: it was shown that dimerization of the RC-LH1-PufX complex from *Rba. sphaeroides* depends on the cytoplasmically exposed N-terminal domain of this transmembrane polypeptide.[6,7] The RC-LH1-PufX dimer adopts a bent configuration that imposes curvature on the membrane bilayer,[8] with far-reaching effects that include the partitioning of the membrane into dimer-rich regions,[9]

Received: August 29, 2013
Revised: September 23, 2013
Published: October 16, 2013

   dx.doi.org/10.1021/bi4011946 | *Biochemistry* 2013, 52, 7575−7585

creation of a favorable environment for stable insertion of the light-harvesting LH2 complex,[10] and, ultimately, the formation of spherical intracytoplasmic membrane vesicles that contain all of the machinery for converting solar energy into ATP. It has been proposed that these 50 nm diameter structures are bacterial organelles,[11] and an atomic-level 3D map of a vesicle has been calculated on the basis of the known membrane locations of the RC-LH1-PufX and LH2 complexes from atomic force microscopy (AFM) studies.[12]

All of the above can be traced back to PufX as a facilitator of quinone/quinol exchange and a driver of dimerization and hence membrane curvature. Here, we report the structure of the dimeric RC-LH1-PufX complex of *Rba. sphaeroides* determined to 8 Å by X-ray crystallography, which deepens our understanding of these roles of PufX. The structure shows that each PufX is positioned adjacent to a RC Q_B site by attachment of its N-terminal region to the cytoplasmic extrinsic domain of RC-H and that both the N- and C-terminal extrinsic regions of PufX promote dimerization by interacting with an LH1 β polypeptide from the other half of the complex. The architecture of the complex creates a channel, allowing Q/QH_2 molecules to cross the LH1 barrier and to internally migrate between the two halves of the dimer structure.

MATERIALS AND METHODS

Purification of the RC-LH1-PufX Complex. The *Rba. sphaeroides* strain DBCΩG,[13] which has neurosporene, hydroxyneurosporene, and methoxyneurosporene as the only carotenoids and which lacks the LH2 complex, was used for the purification of the dimeric RC-LH1-PufX core complex according to previously published methods.[3]

Crystallization and Data Collection. The core dimer complex was concentrated to an optical density of ∼100 at 875 nm and washed several times using a 0.5 mL Vivaspin spin concentrator (100 kDa cutoff) in 9 mM (0.42%) *n*-nonyl-β-D-maltopyranoside (NM) to exchange the purification detergent, *n*-dodecyl-β-D-maltopyranoside (β-DDM). Protein with an absorbance of ∼100 (1 cm path length, 875 nm) was crystallized in a sitting-drop format using the Screenmaker 96 + 8 crystallization robot (Gilson). Crystals grew as plates (500 × 150 × 70 μm) in 14.00% PEG400, 0.10 M *N*-cyclohexyl-3-aminopropanesulfonic acid (CAPS) pH 10.5, and 1.0% spermidine. Crystals were frozen at 100 K, and data were collected at the Science and Technology Facilities Council Synchrotron Radiation Source, Daresbury, on beamline 9.6 with the Area Detector Systems Corporation Quantum 4 detector at a wavelength of 0.912 Å. The crystals diffracted anisotropically between 8.5 and 7.5 Å along the various crystal-axis directions. A data cutoff of 8.0 Å was chosen for the purpose of structure determination, at which resolution I/σ was 1.0, a value usually accepted as the limit of useful data. Data were processed with MOSFLM[14] and merged with SCALA.[15] The crystal space group was $P2_1$, the cell dimensions were a = 78.08 Å, b = 415.07 Å, c = 129.81 Å, and β = 105.75° with a mosaicity of 1.8°, and a data set was processed to an R_{sym} of 9.3% and resolution of 8.0 Å. One dimer was found in the asymmetric unit with the noncrystallographic dimeric axis ∼4° misaligned from the crystallographic a axis.

Molecular Replacement. A molecular replacement (MR) search model of the RC-LH1-PufX dimer complex was derived from EM data.[3,8] The model was composed of the high-resolution RC structure (1PCR) and transmembrane poly-alanine helices representing LH1 $\alpha\beta$ and PufX. Initial MR solutions produced poor electron density maps, especially at the periphery of the complex. Low-resolution EM and AFM images indicate that dimers form V-shaped structures; however, the V angle can vary and depends on the sample preparation or the substrate on which it is placed.[11] To optimize the MR starting model, the relative orientations of monomers were explored by varying two angles (Figure S3A): a rotation angle θ about an axis in the membrane plane "twist" and angle ψ that defines the "bend" angle between monomers (i.e., the V angle). A log likelihood probability function (L) was used in PHASER to calculate the agreement between the observed and calculated structure amplitudes for each model.[16] PHASER was run repeatedly on several dimer models (θ, ψ), and the best L solution occurred at angles θ = 1.5° and ψ = −11.0° (Figure S3A, B). The value for θ is similar or slightly smaller and the ψ angle is significantly lower than the −17.0° found in single-particle reconstruction EM images, which implies that in the X-ray structure the core complex is flattened by comparison.

Electron Density Improvement. Electron density maps were improved by cyclical electron density modification (DM) using solvent flattening, histogram matching, and domain averaging.[17] To prevent model bias from being introduced, the starting model phases were not recombined with DM phases during repeated cycles of the program DM; this allowed the DM phases to evolve independently of the starting model phases. In addition, although the calculated solvent content is 64%, a conservative choice of 40% was used to ensure that structural features were not inadvertently flattened. Limitations arising from data resolution and data completeness can result in noise and termination ripple errors in electron density maps. Solvent flattening and noncrystallographic symmetry (NCS) averaging mitigated some of these effects. Three averaging models were investigated that assumed (1) dimeric NCS only and (2) an NCS domain 'A' comprising reaction centers and 28 NCS 'B' domain repeats comprising LH1 $\alpha\beta$ pairs with associated BChl *a* pigments (Figure S4A). Finally, a third model was considered comprising domain A, a new NCS domain 'C' composed of the two LH1 $\alpha\beta$1 + PufX units, and domain B reassigned to the remaining 26 $\alpha\beta$ LH1 subunits. The phytol chains were removed from BChl *a* molecules because their positions vary between light-harvesting complex structures, for example, in LH2[18] and LH3.[19] The final DM electron density maps have NCS-related correlation coefficients of 0.91 for model 1, 0.9 and 0.70 for model 2 domains A and B, and 0.93, 0.71, and 0.87 for model 3 domains A, B, and C, respectively. The figure of merit increased from 0.31 for the starting model to 0.81 for the final DM phases (Figure S4B). The correlation coefficient for domain B in model 3 suggests that the 26 subunits across both monomers differ slightly around the LH1 ring. Correlation coefficient (CC) statistics between NCS repeats were found to be powerful indicators that structural features were correctly identified, as incorrectly assigned NCS domains result in zero or negative CCs.

Model Fitting to Electron Density. A RC-LH1 dimer was fitted to electron density aided by high-resolution structures of RC (1PCR)[20] and LH2 (1KZU and 1LGH);[18,21] the latter LH2 $\alpha\beta$ repeating units, with chromophores, share significant sequence homology with LH1 $\alpha\beta$ so that BChl *a* pigments can be located in the structure with the correct orientation even though the electron density here is of low resolution. Fitting PufX to the electron density began with a straight α-helix spanning the TM region (30−53) and was thereafter guided by the appearance of new electron density. The starting model of

dx.doi.org/10.1021/bi4011946 | *Biochemistry* 2013, 52, 7575−7585

RC-LH1, used in fitting to electron density, was the MR model. In this model, the RC was mostly intact, whereas the LH1 polypeptides were modeled as 29-residue TM poly alanine chains, and so they were only 40% complete.

The first 2*Fo*−*Fc* map, based on MR phases, showed a strong elongated peak next to LH1 α1, and the electron density around LH1 β1 was reduced and noisy. The provisional interpretation was that the elongated peak was PufX. The old PufX in the starting model was now reassigned to LH1 α1, and the old LH1 α1 was now made into LH1 β1. Side chains were then added to PufX (residues 30−53), and subsequent DM maps revealed new electron density, which was interpreted as PufX (residues 20−31). Additionally, the electron density around LH1 $\alpha\beta$1 improved, indicating that the interpretation of these peptides was a better fit. At this point, side chains were added to all LH1 $\alpha\beta$ peptides with MODELLER[22] using NMR-determined LH1 β[23] and X-ray-determined LH2 polypeptides[18,21] as templates. New DM maps indicated stronger, more connected electron density along LH1 β chains, and, for the first time, turns were revealed at both ends of the α and β chains. Residues were fitted for LH1 α (8−49), LH1 β (1−48), and for PufX density that could accommodate additional residues 2−19, and 54−58 was also found. Refinement (see below) and further rounds of DM calculations resulted in the emergence of density that could be fitted with residues RC-M (302−304) and RC-H (251−260) in the model. LH1 Bchl *a* pigments were repositioned to be consistent with histidines as ligands and were also checked with the position of Bchl *a* in the LH2 $\alpha\beta$ unit from *Phaeospirillum molischianum* superimposed onto an LH1 $\alpha\beta$ unit. Finally, the modeled PufX conformation was compared (see Figure S6B) to an independently determined NMR solution structure of PufX.[24]

Refinement. Refinement was performed in REFMAC5 using tight atomic geometry restraints through an automatically determined matrix weighting between X-ray and geometric terms. Refinement of 38 198 atoms was made against 6308 X-ray measurements and 133 500 geometry restraints. The geometry restraints, which include bond distances, bond angles, torsion, planar, and chiral restraints, cause individual atomic coordinates to be highly correlated locally and so the X-ray and geometry terms are sufficient for stable refinement, albeit mainly on the basis of geometry. The refinement was therefore mostly a geometry regularization process, with the X-ray terms providing statistics on the consistency of the geometry refinement with the X-ray data through the agreement between the X-ray structure factor amplitudes (*Fo*) and atomic model amplitudes (*Fc*). Additional weights were applied to geometry restraints to produce refined rms distance errors between 0.01 and 0.02 Å and rms angle error between 1.0−3.0°. These values are typical of higher-resolution structures, particularly of membrane protein structures. It could be argued that for lower-resolution data this degree of accuracy overconstrains the refinement, but it was judged that the final model should be within the same geometric error levels as obtained for higher-resolution structures. The residues refined were 8−49 for LH1 α chains, 1−48 for LH1 β chains, RC-H 11−260, RC-M 1−304, and RC-L 1−281. It has been shown that the 12 C-terminal residues of PufX are removed by post-translational modification[25] and we found no electron density for residues 59−69 probably because of a disordered conformation of this part of the C-terminal domain. Nevertheless, residues 2−58 represent the majority of the residues in the RC-LH1 dimer. For each NCS monomer, 28 LH1 Bchl *a* pigments, without phytol chains, four RC BChl *a*, two bacteriopheophytin *a*, two ubiquinone, one spheroidene, one phosphate, and one Fe(III) molecule were included in the refinement.

Refinement was performed against data between 20 and 8.0 Å because data below 20 Å suffer from bulk solvent contributions that are not modeled well in refinement programs; this is particularly true of membrane proteins, which also have contributions from detergent micelles. These low-resolution data do not add much to the refinement and even at higher resolution are generally excluded. The possibility of crystal twinning disorder was statistically tested during data processing, which suggested that there could be pseudomerohedral twinning but, because of data resolution and interference from strong NCS symmetry, this was inconclusive. The possibility was reassessed during refinement using the twinning option in REFMAC5, which deconvolutes the data during refinement and so uses corrected structure factor amplitudes for refinement. This refinement indicated a twinning factor $\alpha \approx 0.12$ and resulted in slightly improved refinement statistics compared to twinned data (Table 1). The subsequent electron density maps for twinned and detwinned data were similar and suggest that the small amount of twinning has no major effect on structure determination.

The refinement statistics are comparable with those found for higher-resolution structures. It should be recognized that in most refinements the R_{factor} remains flat and 22% is typical in the resolution range 20−8.0 Å, providing that the model is correct. The good statistics for this structure implies that the model is substantially correct, with the important proviso that the optical resolution is between 5 and 6 Å and that any structural errors (e.g., in side-chain positions) smaller than this will not be seen in the statistics. NCS skews the data intensity distributions toward a number of stronger reflections, which may also account for a low R_{factor}.

Calculation of the 3D Q_B Channel in the Dimeric Core Complex. Interior cavities of the dimer complex were generated using Hollow.[26] Casting of the protein interior cavity was restricted within a cylinder that encompasses the Q_B channel in one-half of the dimeric RC-LH1-PufX complex (d = 10 nm, h = 7 nm). The produced cavity was then sliced, and the edge of each slice was digitized with a spacing step of 1 Å. Areas not belonging to the Q_B channel were removed manually. The Q_B channel in the dimer was then built using Pymol.[27]

Mass Spectrometry-Based Quantification of the Core Complex Subunits: Preparation of ^{15}N-Labeled Internal Standard. Cells (1.5 L) were grown at 37 °C in M9 medium containing $(^{15}NH_4)_2SO_4$ (99 atom %, Cambridge Isotope Laboratories) to an OD of 0.7 at 600 nm and were then transferred to 20 °C for 16 h with 0.4 mM IPTG. Cells were harvested at 4000*g* for 30 min at 4 °C and then resuspended in 20 mL of IMAC binding buffer (25 mM Tris/HCl pH 7.4, 300 mM NaCl, 5 mM imidazole). The cells were broken by sonication (10 × 30 s) on ice, and the lysate was clarified by centrifugation at 33 000*g* for 30 min at 4 °C. The pellet was resuspended in binding buffer and repelleted at 33 000*g* for 30 min at 4 °C. This pellet was resuspended in binding buffer containing 8 M urea and sonicated for a further 10 × 30 s on ice. The resultant solution was stirred for 1 h at 4 °C and subjected to a final centrifugation step at 33 000*g* for 30 min at 20 °C. The supernatant was applied to a 5 mL Ni^{2+}-charged chelating Sepharose column (GE Healthcare) equilibrated in binding buffer containing 8 M urea. The column was washed with 50 mL of binding buffer containing 8 M urea and 50 mL of

dx.doi.org/10.1021/bi4011946 | *Biochemistry* 2013, 52, 7575−7585

Table 1. Data Collection and Refinement Statistics for the RC-LH1-PufX Core Complex Dimer from *Rba. sphaeroides*[a]

data collection	
X-ray source	SRS 9.6
space group	$P2_1$
cell dimensions	
a, *b*, *c* (Å)	78.08
	415.07
	129.81
α, *β*, *γ* (degree)	90.00
	105.75
	90.00
wavelength (Å)	0.912
resolution (Å)	60.8−8.0
	(8.4−8.0)[b]
R_{sym} (%)	9.3 (90.5)
I/σ	5.6 (1.0)
number of reflections	6831
data completeness (%)	82 (80)
multiplicity of reflections	2.9 (2.9)
Refinement Statistics	
resolution range (Å)	20−8.0
number of reflections	6308
number of geometry restraints	133 500
number of atoms	38 198

	twinned	detwinned
twinning factor	NA	0.1174
R_{factor}/R_{free} (%)	23.3/26.4	22.8/25.8
overall correlation coefficient	0.89	0.90
figure of merit	0.84	0.85
bond rms (Å)	0.018	0.013
angle rms (degree)	2.66	2.63
chiral volume rms (Å^3)	0.10	0.08

[a] $R_{sym} = \sum|(I - \langle I\rangle)|/\sum I$, where $\langle I\rangle$ is the average intensity of multiple measurements. R_{factor} and $R_{free} = \sum||Fo| - |Fc||/\sum|Fo|$, where $|Fo|$ and $|Fc|$ are the observed and calculated structure factor amplitudes, respectively. Refinement statistics are given for twinned data and detwinned refinement. Detwinned data were deconvoluted with a twinning factor of 0.1174. [b] Highest-resolution bin.

binding buffer containing 50 mM imidazole and 8 M urea. The ^{15}N-(His_6) protein standard was eluted from the column at 250 mM imidazole and 8 M urea, and its concentration was determined from the calculated molar extinction coefficient at 280 nm (www.expasy.org/protparam/).

Relative Quantification of RC and PufX Proteins. The RC-LH1-PufX complex, prepared as described above in 20 mM HEPES pH 7.8, 100 mM NaCl, 0.03% (w/v) *β*-dodecylmaltoside was buffer-exchanged into digestion buffer (50 mM ammonium bicarbonate (BioUltra, Sigma), 0.05% (w/v) ProteaseMax surfactant (Promega)) in a centrifugal ultrafiltration device (Amicon Ultra, 3 kDa NMWL, Millipore) according to the manufacturer's instructions. Each assay, performed in duplicate, contained 2 μL of the RC-LH1-PufX complex in digestion buffer (10 μg of protein by Bradford assay) and either 10, 20, or 30 pmol of ^{15}N-labeled internal standard protein in a total volume of 16 μL of digestion buffer. One microliter of dithiothreitol (BioUltra, Sigma, 100 mM in digestion buffer) was added followed by incubation at 56 °C for 20 min. S-alkylation was carried out with the addition of 1 μL of iodoacetamide (BioUltra, Sigma, 200 mM in digestion buffer) and incubation in the dark at room temperature for 15 min. Two microliters of trypsin (porcine, dimethylated, proteomics grade, Sigma, 0.2 g/L in digestion buffer) was added, and the proteins were digested at 48 °C for 4 h. A further 2 μL of trypsin (freshly dissolved in digestion buffer) was added followed by incubation at 37 °C for 16 h. To degrade the ProteaseMax surfactant, 2.2 μL of 5% (v/v) trifluoroacetic acid (TFA) was added followed by incubation at room temperature for 5 min. The tryptic peptides were desalted on a C_{18} SpinTip (Proteabio) according to the manufacturer's instructions, dried by vacuum centrifugation, and redissolved in 20 μL of 0.1% (v/v) TFA, 3% (v/v) acetonitrile. Aliquots of 2 μL were analyzed in duplicate by LC−MS/MS using an Ultimate 3000 RSLCnano liquid-chromatography system (Dionex) with 5 mm × 300 μm trapping and 75 μm × 15 cm analytical PepMap C_{18} reverse-phase columns. Tryptic peptide elution was by a 60 min linear gradient from 94% solvent A (0.1% (v/v) formic acid) to 40% solvent B (0.1% (v/v) formic acid, 80% (v/v) acetonitrile) at a flow rate of 300 nL/min.

Stoichiometry Determination of Bacteriochlorophyll *a* and Carotenoid in the RC-LH1-PufX Complex from *Rba. sphaeroides*. The purified core complex (OD 140 at 875 nm, 1 cm path length) was used for the extraction of pigments. Twenty-five microliters of protein solution was mixed with 200 μL of acetone/methanol (7:2, v/v), and the mixture was spun in a desktop centrifuge at 13 000 rpm for 1 min. The supernatant was collected, and the pellet was re-extracted twice with 100 μL of acetone/methanol solvent. All of the collected supernatants were pooled together.

The solvent in the supernatant was removed by gently passing nitrogen gas over the surface of the pooled supernatants, which were kept on ice in the dark. The extracted pigment components, BChl *a*, and the carotenoids neurosporene, hydroxyneurosporene, and methoxyneurosporene were redissolved in 300 μL of methanol, and the absorption spectrum was recorded immediately at room temperature with pure methanol as a baseline. The carotenoids in the methanol solution were extracted using four sequential treatments with 200 μL of hexane, ensuring there was no observable carotenoid in the final hexane layer. The collected hexane solutions were pooled and dried with nitrogen in the dark on ice. The dried carotenoid mixture was dissolved in 300 μL of pure hexane, and its absorption spectrum was recorded at room temperature with pure hexane as a baseline.

To determine if all of the carotenoid had been extracted from the original methanol extract, the hexane extract of carotenoid was dried under nitrogen gas in the dark on ice and then redissolved in 300 μL of methanol. The carotenoid absorbance intensity of this methanol extract was almost the same as the solution before carotenoid extraction. Neurosporene, hydroxyneurosporene, and methoxyneurosporene have the same absorption properties, so the extinction coefficient of neurosporene in hexane at 453 nm,[28] 159 mM^{-1} cm^{-1}, was used for quantification. For BChl *a* in methanol, the extinction coefficient at 770 nm was 76 mM^{-1} cm^{-1};[29] the BChl *a*/neurosporene stoichiometry for the RC-LH1-PufX dimer complex was calculated as 1.06 ± 0.09, consistent with previous extractions of photosynthetic membranes comprising a mixture of LH1 and LH2 complexes[30] and with the extraction of the isolated LH1 complex.[31]

dx.doi.org/10.1021/bi4011946 | *Biochemistry* 2013, 52, 7575−7585

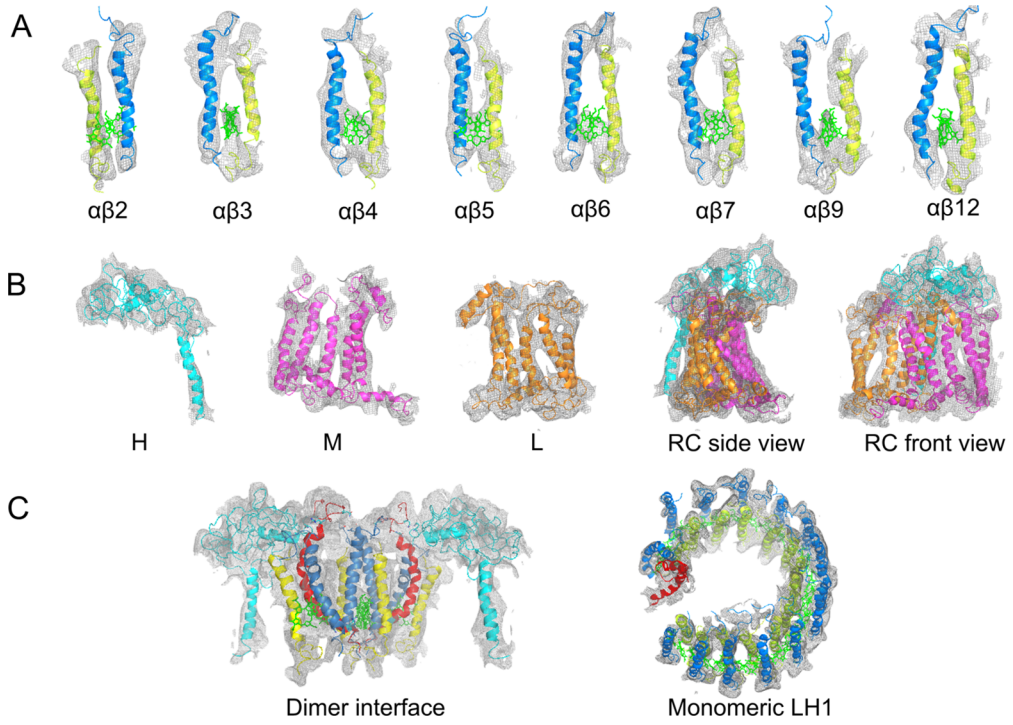

Figure 1. Density maps of selected parts of the RC-LH1-PufX dimer. (A) LH1 $\alpha\beta$ subunits. LH1 α is in yellow, LH1 β, blue, and BChl *a*, bright green, and the electron density is represented by a gray mesh. All LH1 $\alpha\beta$ BChl *a* subunits were fitted into the electron density individually. (B) RC complex. RC-H subunit is in cyan, RC-M, magenta, RC-L, orange, and electron density, gray. The RC complex is viewed from two angles rotated 90° about the *z* axis. (C) On the left, the arrangement of polypeptides at the dimer interface. For the sake of clarity, only the RC-H subunits, the two PufX polypeptides in red, and the 1/1′ and 14/14′ LH1 $\alpha\beta$ pairs are included. On the right, one-half of the dimer with the RC omitted, showing the 14 LH1 $\alpha\beta$ pairs together with a PufX polypeptide. All density maps were produced using Pymol with a contour level of 1.0σ based on the final refined electron density map of the dimer.

RESULTS AND DISCUSSION

Structural Analysis of the RC-LH1-PufX Complex. The RC-LH1-PufX complex was purified from membranes of a LH2-minus mutant of *Rba. sphaeroides*. SDS polyacrylamide gel electrophoresis shows that the RC H, L, and M subunits are present along with the LH1 and PufX polypeptides (Figure S1). To quantify the amount of PufX, we used a MS approach using ^{15}N-labeled internal standards for the RC-M, RC-L, and PufX polypeptides (see Table S1). Proteotypic tryptic peptides derived from the RC-M and -L chains and PufX components of the purified RC-LH1-PufX complex were all in the molar ratio range 0.91−1.22 (Table S2). Thus, the MS analysis confirms that there is one PufX per RC.

The complex was crystallized as described in the Materials and Methods. Figure S2 shows the crystal packing of the RC-LH1-PufX complexes, with neighboring rows of dimers adopting an 'up−down−up' configuration, as seen for 2D crystals of this complex.[3] Thus, these 3D crystals can be regarded as ordered stacks of 2D crystals, with the protruding RC-H subunits in one layer aligned with the slightly recessed periplasmic surface of the next. One consequence of this packing appears to be a reduced curvature of the complex; single-particle reconstruction showed that the two halves of RC-LH1-PufX incline toward each other at an angle of ∼146°, consistent with the 72 nm diameter of dimer-only tubular membranes.[8] However, some flattening has occurred in the 3D lattice, and the angle subtended by the periplasmic face of the complex increases to 158°, indicating some flexibility at the monomer−monomer interface; a similar flattening process was observed when curved native membranes were adsorbed onto a flat mica surface for AFM imaging.[11]

The initial dimer model for molecular replacement was derived from cryo-electron microscopy images of 2D crystals[3] and single-particle reconstruction.[8] This model was composed of the 2.65 Å structure of the RC[20] and polyalanine transmembrane helices for LH1 polypeptides, which were individually fitted into the EM images. The best MR solution for the X-ray data was found by varying two angles that define the relative monomer orientations (Figure S3A,B). The model phases were improved by solvent flattening, histogram matching, and domain averaging (see Figure S4A). The method, described in the Materials and Methods, is identical to the procedure employed for the structure determination of viruses, where structural redundancy is used to overcome limitations of data resolution and data completeness.[32] This high degree of electron density averaging produced good quality electron density maps at 8 Å resolution. The overall quality of the data is reasonable, with an overall R_{sym} of 9% and <5% in the lowest-resolution range (Table 1). It should be noted that the low rms values for bond lengths and bond angles are a reflection of the geometry constraints; they are not absolute coordinate errors. These constraints were used to ensure that the geometry of the model is sensible and that geometry has not been sacrificed to achieve a spuriously low R_{factor}. Given the resolution of our map, the absolute coordinate error is likely to be around 5 to 6 Å. The starting EM-derived model was only 40% complete for LH1, comprising only transmembrane polyalanine chains. Adding side-chains contributed significantly to the electron density, helping to reveal

dx.doi.org/10.1021/bi4011946 | *Biochemistry* 2013, 52, 7575−7585

new features such as N- and C-terminal turns for LH1 and improved density for PufX (see the Materials and Methods for details). However, we emphasize that at this resolution individual side chains could not be resolved from each other in the electron density map; subsequent discussion of the likely interactions between different amino acids relies therefore on the input of various constraints on the final model. Construction and interpretation of this final model was informed not only by data from cryo-electron microscopy, which determined the 8.5 Å projection structure of the complex,[3] but also from single-particle reconstruction,[8] MS analysis (this work), the solution structures of LH1 β and PufX,[7,23,24] the 2.65 Å structure of the reaction center,[20] site-directed-mutagenesis studies of the LH1 complex,[33−35] and the structures of LH2 complexes.[18,21] The resultant R_{factor}/R_{free} values of 22.8/25.8%, can be compared with other structures at this resolution such as the hexameric building block of the HIV capsid (3GV2) (resolution 7.0 Å and R_{factor} 28%)[36] and the staphylococcal complement inhibitor in complex with human complement component C3b (3L5N) (resolution 7.5 Å and R_{factor} 26%).[37]

Overall Architecture of the Complex. Approximately 90% of the entire structure was assigned, sufficient to reveal the overall architecture of this large ~521 kDa complex, which comprises 64 polypeptides, 80 transmembrane helices, and 128 cofactors. Figure 1 shows how the modeled transmembrane helices and extrinsic regions of the RC, LH1, and PufX components fit within the electron densities; a gallery of LH1 $\alpha\beta$ pairs (numbers 2−7, 9, and 12) is displayed on the top row, with LH1 $\alpha\beta$ pairs 1, 8, 10, 11, 13, and 14 also displayed in Figure S5. Figure 1B also shows the fits of the individual RC subunits and the RC complex within the electron density maps. Figure 1C displays the arrangements of RC-H, LH1, and PufX polypeptides at the dimer interface and the curved array of LH1 polypeptides.

Figure 2A,B shows that each RC is surrounded by the LH1 antenna, which comprises an inner ring of 14 LH1 α polypeptides, an outer ring of 14 LH1 β polypeptides, and two BChls sandwiched between each $\alpha\beta$ pair of transmembrane helices. The conformations of the LH1 α and β polypeptides, traced within the electron density map (Figure 1A), adopt a near-perpendicular orientation with respect to the membrane plane. However, the β polypeptides in the outer ring at positions β1 and β1′ (Figure 2C) are different in this respect, having a bent configuration in the region of Trp23, consistent with solution NMR data for LH1 β showing a predominantly helical polypeptide with a more flexible central hinge in the Met19−Trp23 region.[24] Thus, the capacity of LH1 β to flex in this region allows the N-terminal regions of β1 and β1′ to adopt a shape that differs from the majority of LH1 β polypeptides, enabling associations with their respective PufX polypeptides (Figure 2D). The LH1 $\alpha\beta$ units follow the contours of the RC, adopting an elliptical shape that opens outward slightly, allowing quinones to congregate close to the RC Q_B site. Consistent with this, analyses of purified, detergent-washed core dimer complexes show that there are 10−15 ubiquinone molecules and 80−90 phospholipid molecules per RC.[38]

Interactions Between the PufX Polypeptide and the RC-LH Polypeptides within One-Half of the Dimer. Figures 1C (right) and 2D show that there is extra density next to LH1 α1, which is assigned to PufX. Extra transmembrane density in this region was observed in maps

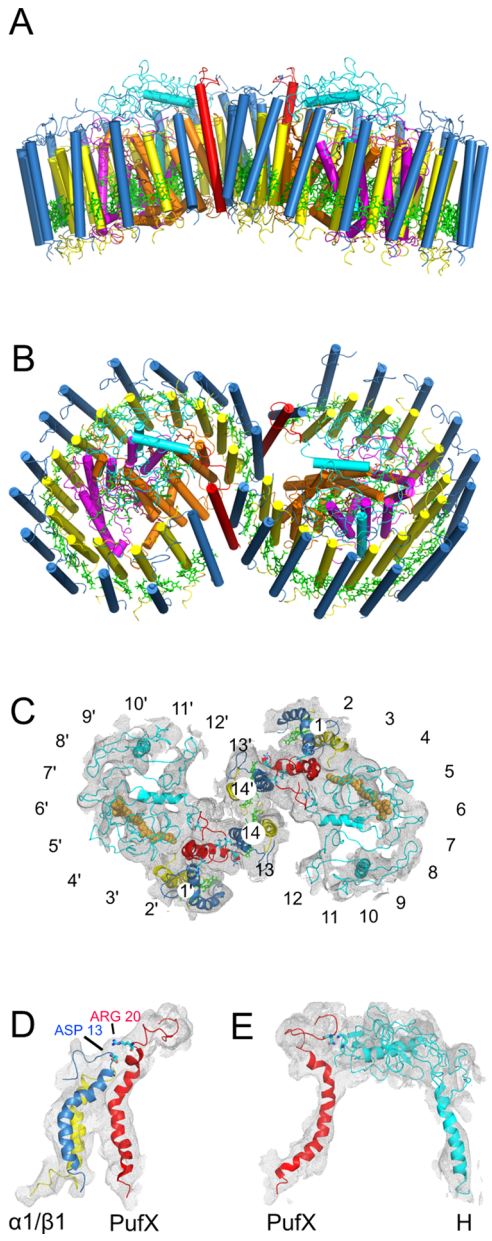

Figure 2. Structure of the RC-LH1-PufX dimer. (A) Complex viewed in the plane of the membrane, with LH1 β in blue, LH1 α in yellow, RC-H in cyan, RC-L in orange, RC-M in magenta, and PufX in red. α-Helices are represented as straight rods. (B) Cytoplasmic face of the complex. (C) Cytoplasmic side of the complex, viewed perpendicular to the membrane with the LH1 subunits in gray and numbered 1−14 on one-half of the dimer and 1′−14′ on the other half. The enclosed gray volume is the electron density for the dimer interface, consisting of the RC-H subunit, the two PufX polypeptides, and the 1/1′ and 14/14′ LH1 $\alpha\beta$ pairs. This represents a view perpendicular to that of the density for the dimer interface in Figure 1C. The RC-bound Q_B quinone (orange), as in 1PCR,[20] shows only 35 carbon atoms of the C50 chain of UQ_{10}. LH1 β1, β1′, β14, and β14′ are in blue, LH1 α1, α1′, α14, and α14′, yellow, the respective LH1 BChl *a* molecules, green, RC-H, cyan, and PufX, red. (D) Side view of the interaction between PufX and the nearest LH1 $\alpha\beta$ pair ($\alpha\beta$1) on the cytoplasmic side of the membrane. (E) Interaction between PufX and RC-H on the cytoplasmic side of the membrane.

calculated using the first MR model. As a final check, 2*Fo*−*Fc* omit maps were calculated using a final model, calculated after cycles of refinement but with LH1 $\alpha\beta$1 and PufX

dx.doi.org/10.1021/bi4011946 | *Biochemistry* 2013, 52, 7575−7585

removed. Figure S6A shows the return of these polypeptides in the electron density map, which is contoured at a 1σ level. The final refined PufX polypeptide chain in our model can be superimposed onto 2NRG, which is a minimized averaged solution structure for PufX in solvent[24] with an rms deviation of 2.08 Å and a maximum Cα atom deviation of 3.75 Å (Figure S6B). The largest deviations are in the region 2−23, where PufX is constrained by interactions with the N-terminal LH1 α-polypeptide and the RC-H chain, consistent with the absence of such constraints in the NMR studies of purified PufX in solvent.[7,24] Although the bend and the N-terminal loop for PufX both closely follow 2NRG (Figure S6B), they were determined completely independently of the NMR structures.[7,24] Furthermore, the position of PufX next to LH1α1 has also been determined independently by cryo-EM (3), although the PufX transmembrane domain is now established as 17 Å from the original best estimate of its position in the EM projection map.[3]

Figure 2C shows the position of PufX and RC-H in relation to the RC Q_B inferred from the RC structure (PDB 1PCR) incorporated into our dimer model. The location of the PufX transmembrane domain is a consequence of the PufX-RC-H interaction and the association of PufX with the bent LH1 β1 polypeptide. PufX prevents the LH1 array from completely surrounding the RC, creating a channel (Figure 5B) that allows the traffic of quinones and quinols as they shuttle between the Q_B site, the external quinone pool, and the cytochrome bc_1 complex. A similar situation is envisaged for the RC-LH1-PufW complex of *Rhodopseudomonas palustris*;[2] Figure S7A,B shows a comparison between the *Rba. sphaeroides* dimer and *Rps. palustris* monomer complexes, aligned using the *Rba. sphaeroides* RC that is modeled into both structures. Figure S7B shows the relative positions of PufX and W in relation to the RC Q_B site; the minimum center-to-center distance between the transmembrane helices is ∼5 Å.

Figure 2D shows that PufX is stabilized by close contacts with the N-termini of LH1 α1 and β1 on the cytoplasmic side of the membrane. PufX is also intimately associated with the extrinsic domain of the RC-H subunit (Figure 2E), with PufX residues 21−30 running parallel with the RC-H C-terminal region, which forms a bend at residues 244−246. The last 10 residues of RC-H are usually missing in RC X-ray structures but are observed in 2J8D,[39] where the residues 228−257 are α-helical with a bend at 244−245. Our structure is consistent with this, but a greater bend has been modeled into RC-H in this region to follow the electron density and contours of PufX. The absence of PufX from all RC crystal structures may explain why this otherwise flexible C-terminal region is not usually observed in electron density maps. The attachment of PufX to RC-H through residues on the cytoplasmic faces of these proteins is consistent with AFM nanodissection experiments where removal of RC-H was frequently seen in PufX-minus mutants.[10] This association between RC-H and PufX forms a likely start signal for the assembly of the RC-LH1-PufX complex by forming an arch with RC-H that prevents blockage of the passage to the RC Q_B site and also provides an anchoring point for docking the first LH1 $\alpha_1\beta_1$BChl$_2$ subunit onto PufX. Encirclement of the RC could then proceed by the addition of more LH1 $\alpha\beta$BChl$_2$ units. This assembly sequence was originally proposed on the basis of Western blotting experiments where the RC-H subunit was detectable first followed by PufX and then the LH1 α and β polypeptides.[40]

Interactions Involving PufX That Stabilize Formation of the Core Dimer Complex. A third set of interactions, between the N- and C-terminal extrinsic regions of PufX and the LH1 β14′ polypeptide, stabilizes formation of the dimer. In our model, at the cytoplasmic face of the complex, Asn12 of PufX on one-half of the dimer is predicted to approach a region of LH1 β14′ on the other half that includes Asp13 (Figure 3A). This prediction is consistent with results from a series of

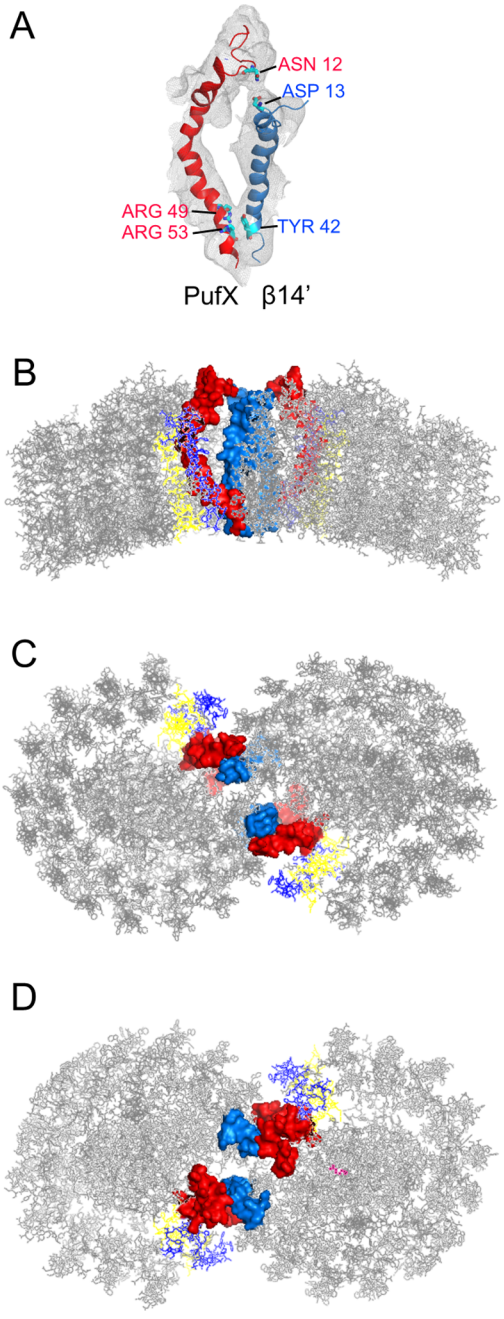

Figure 3. PufX interactions that stabilize the RC-LH1-PufX dimer. (A) Interactions between the N- and C-terminal extrinsic regions of PufX on one-half of the dimer and the 14th LH1β polypeptide from the other half of the complex. (B) RC-LH1-PufX dimer structure in gray viewed from the membrane plane, with the two PufX polypeptides (red) and the LH1 β14 and β14′ highlighted. LH1 β1 and β1′ are in blue and LH1 α1 and α1′ are in yellow. (C) Cytoplasmic side of the complex. (D) Periplasmic side of the complex.

dx.doi.org/10.1021/bi4011946 | *Biochemistry* 2013, 52, 7575−7585

deletions constructed at the N-terminus of PufX, where truncation of 12 or more residues from the N-terminus abolished dimerization of the complex.[6,7] The structure also shows an association between the C-terminal regions of PufX and β14′, consistent with the effects of C-terminal truncation of PufX.[6] The resolution of the structure does not allow precise assignments of contacts between polypeptides, but two PufX residues, Arg49 and Arg53, are found in this C-terminal contact zone, and alteration of both of these residues to Leu abolishes dimer formation, leaving the levels of PufX unaffected.[41] The association between RC-LH1-PufX monomers is likely to be relatively weak because photosynthetic membranes contain some monomers.[42] Figure 3B–D shows three views of the dimer structure with only the two PufX polypeptides (red) and the LH1 β14 and β14′ highlighted, which emphasize the importance of both the N- and C-terminal regions of PufX for promoting dimerization of the complex.

Pigments within the RC-LH1-PufX Dimer Complex. Figure 4A,B shows all 56 LH1 BChls together with the 8 BChls,

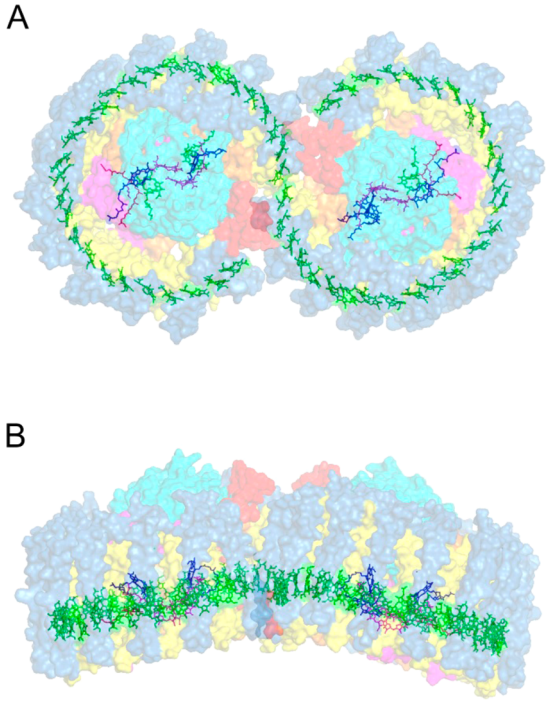

Figure 4. LH1 and RC pigments in the RC-LH1-PufX dimer complex. (A) LH1 BChl *a* pigments (green) enclosing the RC cofactors, viewed perpendicular to the membrane plane from cytoplasmic side. For clarity, only the BChl special pair (purple), accessory BChl a (green), Bphe *a* (blue), and carotenoid (pink) are shown for the RC cofactors. The phytol tails of the LH1 BChls are not shown. To highlight the position of the pigment molecules in the protein, 30% transparency was imposed on the dimer model. The colors for LH1, PufX and RC polypeptides are as in Figure 2A,B. (B) RC-LH1-PufX dimer complex, again with 30% transparency imposed, showing the horizontal alignment of the LH1 BChl *a* molecules with the RC pigments.

4Bph, and 2 carotenoid pigments contributed by the two RCs, assigned here on the basis of the crystallographic structure of the *Rba. sphaeroides* RC complex[20] modeled into the dimer structure. There are no LH1 carotenoids included in Figure 4 because of the low resolution of the electron density map, but pigment extractions (see the Materials and Methods) show that there is one carotenoid for every LH1 BChl, possibly accounting for the extraordinary photostability of this complex when spheroidenone is bound.[43,44] The disc-like electron densities for 8 of the 14 LH1 $\alpha\beta$ pairs in Figure 1A and for the rest of the pairs in Figure S5 allow an approximate positioning of the LH1 BChls. The precise positions and orientations of the LH1 BChls in the structural model could not be assigned on the basis of the 8 Å X-ray data, and instead we took into account results from site-directed mutagenesis of the C-terminal aromatic residues α43Trp (α +11 in relation to the conserved His0 ligand) and βTrp47 (β +9), altered to Phe in each case.[34,35] Resonance Raman spectroscopy of the mutant complexes had shown that each of these mutations breaks a hydrogen bond to the C3-acetyl carbonyl group on each of the BChls. It was therefore proposed that the LH1 α- and β-bound BChls within a minimal LH1 unit were hydrogen–bonded to αTrp 43 and βTrp47, respectively,[34] which necessitates a bend in the vicinity of αPro39. Further mutagenesis/Raman experiments established that the LH1 BChls are ligated to the conserved histidine (His0) residues.[33] The assignments of 56 LH1 $\alpha\beta$ histidines as BChl ligands and 56 H–bonds from C-terminal LH1 residues to C3-acetyl carbonyls of LH1 BChls provided important constraints for constructing the final model of the RC-LH1-PufX complex, as did spectroscopic studies such as the linear dichroism data for the isolated LH1 complex.[45] Finally, the homology of LH1 and LH2 with respect to His ligands and hydrogen bonding of C3-acetyl carbonyls enabled a check of BChl position by superimposition of the high-resolution LH2 structures.[18,21]

The angle made by the two arcs of LH1 BChls is clearly seen in Figure 4B, as is the horizontal alignment of the LH1 BChls with the RC special pair of BChls, which are the site of primary photochemistry. This alignment is consistent with an earlier AFM study.[46] Figure 4A shows how the 56 LH1 BChls snake around the RC pigments. The average distance from each LH1 α BChl Mg atom to a point bisecting the Mg–Mg pair of the RC $BChl_2$ dimer is 47 ± 2 Å; excitation energy transfer from LH1 BChls to the RC special pair has a time constant of 37 ps at 77 K,[47] complying with this relatively large separation. This is a relatively long time scale in the context of, for example, LH2 to LH1 transfers, which are almost an order of magnitude shorter,[48] but it has been proposed that a closer approach of the LH1 BChls would risk photooxidation of the antenna pigments by the RC special pair.[49] The close approach of the LH1 $\alpha\beta$14 and $\alpha\beta$14′ subunits creates the conditions for the migration of excited states among all 56 LH1 BChls, consistent with measurements of fluorescence yield in isolated dimeric complexes that show a high degree of energy transfer connectivity between the two halves of the complex.[50] Excitation sharing between the RCs[50,51] could help to maintain efficient charge separation under high light conditions, allowing energy to migrate rapidly from the half of the dimer with an already photooxidized ('closed') RC to an 'open' RC. PufX-mediated dimerization leads to enlargement and curvature of the complex, which promotes self-association of dimers, as predicted by Monte Carlo simulations of protein crowding.[9] Although in principle the excitation energy can rapidly access all of the RCs within an array of dimers, fluorescence yield measurements found no evidence for interdimer energy transfer.[50]

Identification of a Putative Quinone Channel within the Dimer Complex. The turnover of RC photochemistry requires the constant exchange of quinones and quinols across the apparent barrier imposed by the LH1 complex. To visualize

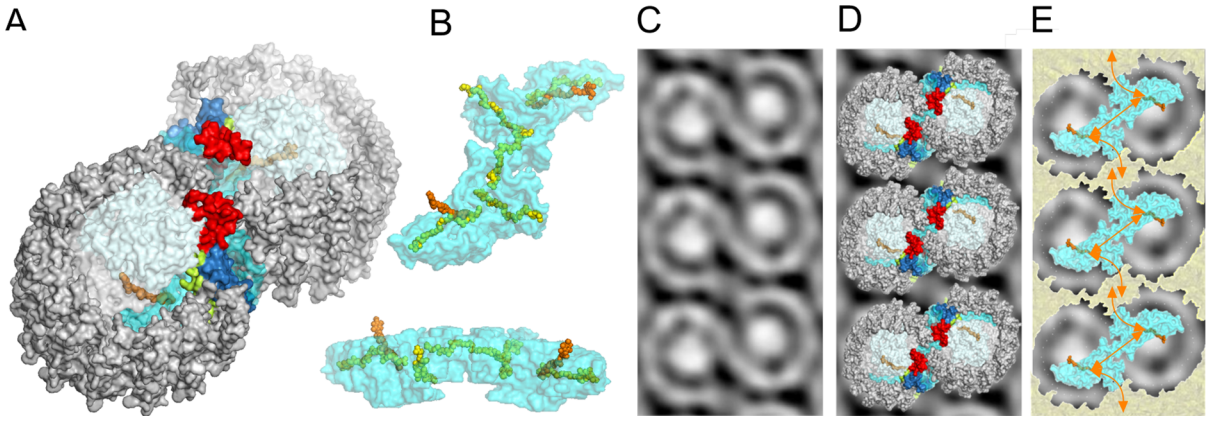

Figure 5. Continuous 3D space enclosed by the LH1 complex. (A) Structure of the RC-LH1-PufX dimer from the cytoplasmic side with RC and LH1 subunits in gray, except for LH1 β1 and 1′ in blue, and LH1 α1 and 1′ in yellow; PufX is in red. The RC subunits are semitransparent so that Q_B, in orange, can be seen. The cyan coloring represents the continuous 3D space enclosed by the LH1 ring that communicates with the exterior of the complex and with the other half of the dimer. (B) Views of the 3D space in panel A but with all proteins removed and with the two Q_B molecules (orange) from 1PCR[20] retained; five additional quinones (yellow), modeled as full-length UQ_{10} molecules (from 2GMR), are shown to demonstrate that the 3D space is sufficient to enclose several such quinones. The top view is in the same orientation as in panel A; the lower view is from the side of the complex, parallel to the membrane plane. (C) Negatively stained EM projection map of a natural membrane from a RC-LH1-PufX dimer-only mutant of *Rba. sphaeroides* showing the packing of adjacent dimer complexes into rows.[8] (D) Superposition of three RC-LH1-PufX dimers onto the EM image. Each dimer complex was positioned manually by aligning the gap in the LH1 ring seen in panel C with the gap between LH1 β14 and 14′ and the neighboring LH1 ring from the other half of the complex, as in Qian et al.[3] (E) Schematic diagram showing possible pathways for quinone diffusion in, out, and through the dimer structures.

a possible channel allowing the external quinone pool access to the RC Q_B site, we calculated the continuous 3D space enclosed by the LH1 ring. This 3D volume, represented in blue in Figure 5A,B shows that there is indeed continuity between the external membrane environment and the RC Q_B site, with sufficient room within this volume to accommodate several quinone molecules, modeled as the full-length molecules with a C50 tail, rather than the C35 in the 1PCR RC structure.[20] The lack of structural resolution and their inherent disorder precludes any direct observation of the sequestered lipids and quinones, but their presence within this 3D volume can be inferred from extractions of purified core dimers that revealed 10−15 ubiquinone molecules and 80−90 phospholipid molecules per RC.[38] The projection structure from cryo-EM[3] also showed a space between the LH1 ring and the RC, and the diffuse density for the first LH1 β polypeptide (now β1 but originally numbered β14 in ref 3) was proposed to reflect a highly mobile region of the complex. In this projection map, the LH1 $\alpha\beta$1 polypeptide pair has shifted outward from the RC by up to 7 Å relative to its position in Figures 2C and 3B−D, widening the LH1 arc and enclosing a space significantly larger than that represented in Figure 5A,B, providing even more room for sequestering and exchange of quinones. Thus, Figures 2−5 probably depict one of several conformational states of this dimeric complex, consistent with AFM experiments showing that the LH1 ring is inherently flexible.[52] In bacteria with PufX, this polypeptide prevents ring closure, holding LH1 subunits in an open, dynamically variable state to promote the exchange of quinones with the external pool. Kinetic studies of purified dimeric core complexes examined the effects of inhibiting a variable fraction of RCs with stigmatellin and provided evidence for quinone sharing by the two RCs within a dimer.[50] The 3D volume in Figure 5A,B provides a structural basis for this observation and raises the possibility that quinones can cross between the two halves of the structure. Photosynthetic membranes were proposed to contain confined, quinone-rich regions surrounding RC-LH1-PufX dimers;[50] Figure 5C,D shows how the association of two or more RC-LH1-PufX dimers, as seen in AFM and EM images of photosynthetic membranes,[8,42] could create such regions and raises the possibility that migration within and between dimers (Figure 5E; also, see the movie in the Supporting Information) could fast-track quinols to their destination, the cytochrome bc_1 complex, further optimizing the ability of *Rba. sphaeroides* to harvest and utilize light energy.

■ ASSOCIATED CONTENT

Ⓢ Supporting Information

SDS polyacrylamide gel electrophoresis of the RC-LH1-PufX complex; crystal packing of the RC-LH1-PufX complexes; structure determination of the RC-LH1-PufX dimer: variation of angles between monomers and NCS domain definitions for electron density averaging; density maps for all 14 LH1 $\alpha\beta$ subunits within the RC-LH1-PufX dimer; omit maps showing the return into the electron density map of PufX, the LH1 α1 and β1 polypeptides, and the BChls; superimposed structures of PufX from the electron density map and from the solution structure determined by NMR; structural comparison between the RC-LH1-PufX dimer complex from *Rba. sphaeroides* with the RC-LH1-PufW monomer complex from *Rps. palustris*; mass spectrometry-based quantification of the core complex subunits: preparation of ^{15}N-labeled internal standards and relative quantification of RC and PufX proteins; and movie of quinone migration across the LH1 ring to the RC Q_B site followed by quinol migration to the other half of the complex. This material is available free of charge via the Internet at http://pubs.acs.org.

Accession Codes

Coordinates and structure factors have been deposited in the Protein Data Bank and are split between the entries 4JC9 and 4JCB.

AUTHOR INFORMATION

Corresponding Author

*E-mail: c.n.hunter@sheffield.ac.uk. Phone: +441142224191.

Author Contributions

‖These authors contributed equally.

Funding

P.Q., M.Z.P., P.J.J., A.A.B., J.D.O, M.J.D, P.A.B., and C.N.H. gratefully acknowledge funding from the Biotechnology and Biological Sciences Research Council (U.K.) and Science and Technology Facilities Council. C.N.H. and A.A.B. were also supported as part of the Photosynthetic Antenna Research Center (PARC), an Energy Frontier Research Center funded by the U.S. Department of Energy, Office of Science, and Office of Basic Energy Sciences under award no. DE-SC0001035.

Notes

The authors declare no competing financial interest.

ABBREVIATIONS USED

AFM, atomic force microscopy; BChl *a*, bacteriochlorophyll *a*; CAPS, *N*-cyclohexyl-3-aminopropanesulfonic acid; DM, density modification; *β*-DDM, *n*-dodecyl-*β*-D-maltopyranoside; EM, electron microscopy; LH, light harvesting; MR, molecular replacement; NM, *n*-nonyl-*β*-D-maltopyranoside; NMR, nuclear magnetic resonance; RC, reaction center

REFERENCES

(1) Bullough, P. A., Qian, P., and Hunter, C. N. (2008) Reaction center-light harvesting core complexes of purple bacteria, in *The Purple Phototrophic Bacteria* (Hunter, C. N., Daldal, F., Thurnauer, M. C., and Beatty, J. T., Eds.), pp 155−179, Springer, Dordrecht.

(2) Roszak, A. W., Howard, T. D., Southall, J., Gardiner, A. T., Law, C. J., Isaacs, N. W., and Cogdell, R. J. (2003) Crystal structure of the RC-LH1 core complex from *Rhodopseudomonas palustris*. *Science 302*, 1969−1972.

(3) Qian, P., Hunter, C. N., and Bullough, P. A. (2005) The 8.5 Å projection structure of the core RC-LH1-PufX dimer of *Rhodobacter sphaeroides*. *J. Mol. Biol. 349*, 948−960.

(4) Farchaus, J. W., Gruenberg, H., and Oesterhelt, D. (1990) Complementation of a reaction center-deficient *Rhodobacter sphaeroides pufLMX* deletion strain in *trans* with *pufBALM* does not restore the photosynthesis-positive phenotype. *J. Bacteriol. 172*, 977−985.

(5) Lilburn, T. G., Haith, C. E., Prince, R. C., and Beatty, J. T. (1992) Pleiotropic effects of *pufX* gene deletion on the structure and function of the photosynthetic apparatus of *Rhodobacter capsulatus*. *Biochim. Biophys. Acta 1100*, 160−170.

(6) Francia, F., Wang, J., Zischka, H., Venturoli, G., and Oesterhelt, D. (2002) Role of the N- and C-terminal regions of the PufX protein in the structural organization of the photosynthetic core complex of *Rhodobacter sphaeroides*. *Eur. J. Biochem. 269*, 1877−1885.

(7) Ratcliffe, E. C., Tunnicliffe, R. B., Ng, I. W., Adams, P. G., Qian, P., Holden-Dye, K., Jones, M. R., Williamson, M. P., and Hunter, C. N. (2011) Experimental evidence that the membrane-spanning helix of PufX adopts a bent conformation that facilitates dimerisation of the *Rhodobacter sphaeroides* RC-LH1 complex through N-terminal interactions. *Biochim. Biophys. Acta 1807*, 95−107.

(8) Qian, P., Bullough, P., and Hunter, C. N. (2008) Three-dimensional reconstruction of a membrane-bending complex. *J. Biol. Chem. 283*, 14002−14011.

(9) Frese, R. N., Pàmies, J. C., Olsen, J. D., Bahatyrova, S., van der Weij-de Wit, C. D., Aartsma, T. J., Otto, C., Hunter, C. N., Frenkel, D., and van Grondelle, R. (2008) Protein shape and crowding drive domain formation and curvature in biological membranes. *Biophys. J. 94*, 640−647.

(10) Adams, P. G., Mothersole, D. J., Ng, I. W., Olsen, J. D., and Hunter, C. N. (2011) Monomeric RC-LH1 core complexes retard LH2 assembly and intracytoplasmic membrane formation in PufX-minus mutants of *Rhodobacter sphaeroides*. *Biochim. Biophys. Acta 1807*, 1044−1055.

(11) Tucker, J. D., Siebert, C. A., Escalante, M., Adams, P. G., Olsen, J. D., Otto, C., Stokes, D. L., and Hunter, C. N. (2010) Membrane invagination in *Rhodobacter sphaeroides* is initiated at curved regions of the cytoplasmic membrane, then forms both budded and fully detached spherical vesicles. *Mol. Microbiol. 76*, 833−847.

(12) Sener, M. K., Olsen, J. D., Hunter, C. N., and Schulten, K. (2007) Atomic-level structural and functional model of a bacterial photosynthetic membrane vesicle. *Proc. Natl. Acad. Sci. U.S.A. 104*, 15723−15728.

(13) Jones, M. R., Fowler, G. J. S., Gibson, L. C. D., Grief, G. G., Olsen, J. D., Crielaard, W., and Hunter, C. N. (1992) Mutants of *Rhodobacter sphaeroides* lacking one or more pigment-protein complexes and complementation with reaction-centre, LH1, and LH2 genes. *Mol. Microbiol. 6*, 1173−1184.

(14) Leslie, A. G. W. (1999) Integration of macromolecular diffraction data. *Acta Crystallogr., Sect. D 55*, 1696−1702.

(15) Winn, M. D., Ballard, C. C., Cowtan, K. D., Dodson, E. J., Emsley, P., Evans, P. R., Krissinel, E. B., Leslie, A. G. W., McCoy, A., McNicholas, S. J., Murshudov, G. N., Pannu, N. S., Potterton, E. A., Powell, H. R., Read, R. J., Vagin, A., and Wilson, K. S. (2011) Overview of the CCP4 suite and current developments. *Acta Crystallogr., Sect. D 67*, 235−242.

(16) McCoy, A. J., Grosse-Kunstleve, R. W., Adams, P. D., Winn, M. D., Storoni, L. C., and Read, R. J. (2007) Phaser crystallographic software. *J. Appl. Crystallogr. 40*, 658−674.

(17) Cowtan, K., and Main, P. (1998) Miscellaneous algorithms for density modification. *Acta Crystallogr., Sect. D 54*, 487−493.

(18) McDermott, G., Prince, S. M., Freer, A. A., Hawthornthwaite-Lawless, A. M., Papiz, M. Z., Cogdell, R. J., and Isaacs, N. W. (1995) Crystal structure of an integral membrane light-harvesting complex from photosynthetic bacteria. *Nature 374*, 517−521.

(19) McLuskey, K., Prince, S. M., Cogdell, R. J., and Isaacs, N. W. (2001) The crystallographic structure of the B800−820 LH3 light-harvesting complex from the purple bacteria *Rhodopseudomonas acidophila* strain 7050. *Biochemistry 40*, 8783−8789.

(20) Ermler, U., Fritzsch, G., Buchanan, S. K., and Michel, H. (1994) Structure of the photosynthetic reaction centre from *Rhodobacter sphaeroides* at 2.65 Å resolution: Cofactors and protein-cofactor interactions. *Structure 2*, 925−936.

(21) Koepke, J., Hu, X. C., Muenke, C., Schulten, K., and Michel, H. (1996) The crystal structure of the light-harvesting complex II (B800-B850) from *Rhodospirillum molischanum*. *Structure 4*, 581−597.

(22) Sali, A., and Blundell, T. L. (1993) Comparative protein modeling by satisfaction of spatial restraints. *J. Mol. Biol. 234*, 779−815.

(23) Conroy, M. J., Westerhuis, W. H., Parkes-Loach, P. S., Loach, P. A., Hunter, C. N., and Williamson, M. P. (2000) The solution structure of *Rhodobacter sphaeroides* LH1*β* reveals two helical domains separated by a more flexible region: Structural consequences for the LH1 complex. *J. Mol. Biol. 298*, 83−94.

(24) Tunnicliffe, R. B., Ratcliffe, E. C., Hunter, C. N., and Williamson, M. P. (2006) The solution structure of the PufX polypeptide from *Rhodobacter sphaeroides*. *FEBS Lett. 580*, 6967−6971.

(25) Parkes-Loach, P. S., Law, C. J., Recchia, P. A., Kehoe, J., Nehrlich, S., Chen, J., and Loach, P. A. (2001) Role of the core region of the PufX protein in inhibition of reconstitution of the core light-harvesting complexes of *Rhodobacter sphaeroides* and *Rhodobacter capsulatus*. *Biochemistry 40*, 5593−5601.

(26) Ho, B. K., and Gruswitz, F. (2008) HOLLOW: Generating accurate representations of channel and interior surfaces in molecular structures. *BMC Struct. Biol 8*, 49−54.

(27) DeLano, W. L. (2002) *The PyMOL Molecular Graphics System*, DeLano Scientific Inc., San Carlos, CA.

(28) Sashima, T., Koyama, Y., Yamada, T., and Hashimoto, H. (2000) The $1B_u^+$, $1B_u^-$, and $2A_g^-$ energies of crystalline lycopene, *β*-carotene, and mini-9-*β*-carotene as determined by resonance-Raman

excitation profiles: Dependence of the $1B_u^-$ state energy on the conjugation length. *J. Phys. Chem. B 104*, 5011−5019.
(29) Clayton, R. K. (1966) Spectroscopic analysis of bacteriochlorophylls in vitro and in vivo. *Photochem. Photobiol. 5*, 669−677.
(30) Sistrom, W. R. (1978) Control of Antenna Pigment Components, in *The Photosynthetic Bacteria* (Clayton, R. K. and Sistrom, W. R., Eds.) pp 841−848, Plenum, New York.
(31) Broglie, R. M., Hunter, C. N., Delepelaire, P., Niederman, R. A., Chua, N.-H., and Clayton, R. K. (1980) Isolation and characterization of the pigment-protein complexes of *Rhodopseudomonas sphaeroides* by lithium dodecyl sulfate polyacrylamide gel electrophoresis. *Proc. Natl. Acad. Sci. U.S.A. 77*, 87−91.
(32) Grimes, M., Burroughs, J. N., Gouet, P., Diprose, J. M., Malby, R., Zientara, S., Mertens, P. P., and Stuart, D. I. (1998) The atomic structure of the bluetongue virus core. *Nature 395*, 470−478.
(33) Olsen, J. D., Sturgis, J. N., Westerhuis, W. H., Fowler, G. J. S., Hunter, C. N., and Robert, B. (1997) Site-directed modification of the ligands to the bacteriochlorophylls of the light-harvesting LH1 and LH2 complexes of *Rhodobacter sphaeroides*. *Biochemistry 36*, 12625−12632.
(34) Sturgis, J. N., Olsen, J. D., Robert, B., and Hunter, C. N. (1997) Functions of conserved tryptophan residues of the core light-harvesting complex of *Rhodobacter sphaeroides*. *Biochemistry 36*, 2772−2778.
(35) Olsen, J. D., Sockalingum, G. D., Robert, B., and Hunter, C. N. (1994) Modification of a hydrogen bond to a bacteriochlorophyll *a* molecule in the light harvesting 1 antenna of *Rhodobacter sphaeroides*. *Proc. Natl. Acad. Sci. U.S.A. 91*, 7124−7128.
(36) Pornillos, O., Ganser-Pornillos, B. K., Kelly, B. N., Hua, Y. Z., Whitby, F. G., Stout, C. D., Sundquist, W. I., Hill, C. P., and Yeager, M. (2009) X-ray structures of the hexameric building block of the HIV capsid. *Cell 137*, 1282−1292.
(37) Garcia, B. L., Ramyar, K. X., Tzekou, A., Ricklin, D., McWhorter, W. J., Lambris, J. D., and Geisbrecht, B. V. (2010) Molecular basis for complement recognition and inhibition determined by crystallographic studies of the staphylococcal complement inhibitor (SCIN) bound to C3c and C3b. *J. Mol. Biol. 402*, 17−29.
(38) Dezi, M., Francia, F., Mallardi, A., Colafemmina, G., Palazzo, G., and Venturoli, G. (2007) Stabilization of charge separation and cardiolipin confinement in antenna-reaction center complexes purified from *Rhodobacter sphaeroides*. *Biochim. Biophys. Acta 1767*, 1041−1056.
(39) Koepke, J., Krammer, E. M., Klingen, A. R., Sebban, P., Ullmann, G. M., and Fritzsch, G. (2007) pH modulates the quinone position in the photosynthetic reaction center from *Rhodobacter sphaeroides* in the neutral and charge separated states. *J. Mol. Biol. 371*, 396−409.
(40) Pugh, R. J., McGlynn, P., Jones, M. R., and Hunter, C. N. (1998) The LH1-RC core complex of *Rhodobacter sphaeroides*: Interaction between components, time-dependent assembly, and topology of the PufX protein. *Biochim. Biophys. Acta 1366*, 301−316.
(41) Ng, I. W. (2008) A structural and functional study of the RC-LH1-PufX core complex from *Rhodobacter sphaeroides*, Ph.D. Thesis, University of Sheffield, Sheffield, United Kingdom.
(42) Bahatyrova, S., Frese, R. N., Siebert, C. A., Olsen, J. D., van der Werf, K. O., van Grondelle, R., Niederman, R. A., Bullough, P. A., Otto, C., and Hunter, C. N. (2004) The native architecture of a photosynthetic membrane. *Nature 430*, 1058−1062.
(43) Magis, G. J., Olsen, J. D., Reynolds, N. P., Leggett, G. J., Hunter, C. N., Aartsma, T. J., and Frese, R. N. (2011) Use of engineered unique cysteine residues to facilitate oriented coupling of proteins directly to a gold substrate. *Photochem. Photobiol. 87*, 1050−1057.
(44) Šlouf, V., Chabera, P., Olsen, J. D., Martin, E. C., Qian, P., Hunter, C. N., and Polivka, T. (2012) Photoprotection in a purple phototrophic bacterium mediated by oxygen-dependent alteration of carotenoid excited-state properties. *Proc. Natl. Acad. Sci. U.S.A. 109*, 8570−8575.
(45) Kramer, H. J. M., Pennoyer, J. D., van Grondelle, R., Westerhuis, W. H. J., Niederman, R. A., and Amesz, J. (1984) Low-temperature optical properties and pigment organization of the B875 light-harvesting bacteriochlorophyll-protein complex of purple photosynthetic bacteria. *Biochim. Biophys. Acta 767*, 335−344.
(46) Fotiadis, D., Qian, P., Philippsen, A., Bullough, P. A., Engel, A., and Hunter, C. N. (2004) Structural analysis of the reaction center light-harvesting complex I photosynthetic core complex of *Rhodospirillum rubrum* using atomic force microscopy. *J. Biol. Chem. 279*, 2063−2068.
(47) Visscher, K. J., Bergström, H., Sundström, V., Hunter, C. N., and van Grondelle, R. (1989) Temperature dependence of energy-transfer from the long wavelength antenna BChl-896 to the reaction center in *Rhodospirillum rubrum, Rhodobacter sphaeroides* (w.t. and M21 mutant) from 77 to 177K, studied by picosecond absorption spectroscopy. *Photosynth. Res. 22*, 211−217.
(48) Hess, S., Chachisvilis, M., Timpmann, K., Jones, M. R., Fowler, G. J. S., Hunter, C. N., and Sundström, V. (1995) Temporally and spectrally resolved subpicosecond energy transfer within the peripheral antenna complex (LH2) and from LH2 to the core antenna complex in photosynthetic purple bacteria. *Proc. Natl. Acad. Sci. U.S.A. 92*, 12333−12337.
(49) Noy, D., Moser, C. C., and Dutton, P. L. (2006) Design and engineering of photosynthetic light-harvesting and electron transfer using length, time, and energy scales. *Biochim. Biophys. Acta 1757*, 90−105.
(50) Comayras, R., Jungas, C., and Lavergne, J. (2005) Functional consequences of the organization of the photosynthetic apparatus in *Rhodobacter sphaeroides*. I. Quinone domains and excitation transfer in chromatophores and reaction center center antenna complexes. *J. Biol. Chem. 280*, 11203−11213.
(51) Sener, M., Hsin, J., Trabuco, L. G., Villa, E., Qian, P., Hunter, C. N., and Schulten, K. (2009) Structural model and excitonic properties of the dimeric RC-LH1-PufX complex from *Rhodobacter sphaeroides*. *Chem. Phys. 357*, 188−197.
(52) Bahatyrova, S., Frese, R. N., van der Werf, K. O., Otto, C., Hunter, C. N., and Olsen, J. D. (2004) Flexibility and size heterogeneity of the LH1 light harvesting complex revealed by atomic force microscopy: functional significance for bacterial photosynthesis. *J. Biol. Chem. 279*, 21327−21333.